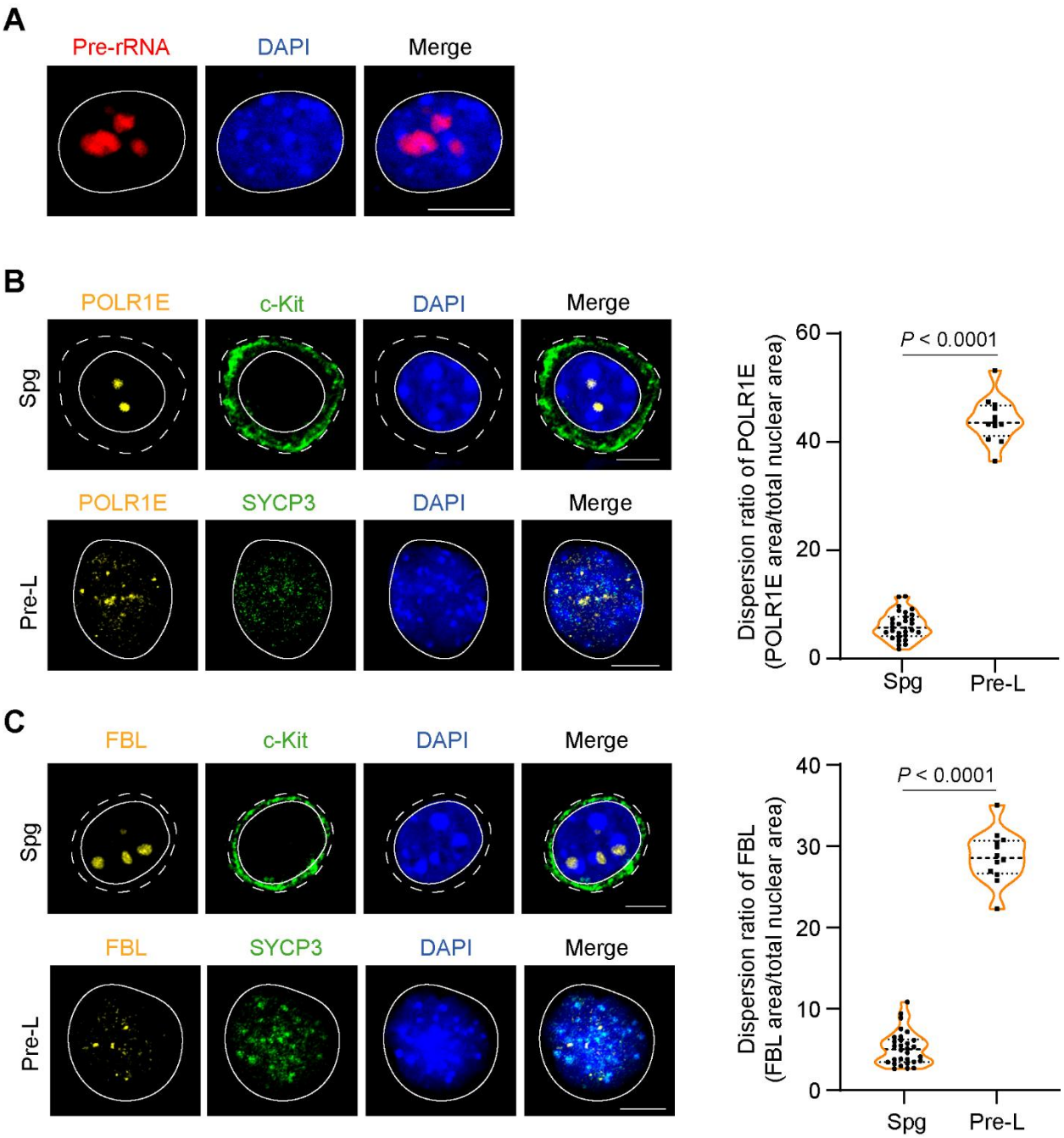

Figure S1 Nucleolar components in the spermatocytes and MEFs.

(A) Examination of the pre-rRNA in MEFs.

(B, C) Examination of the nucleolar proteins POLR1E **(B)** and FBL **(C)** in spermatogonia (c-Kit+) and pre-leptotene spermatocytes (SYCP3+). Representative images are shown at left. Nuclei were counterstained with DAPI (blue). Spg, spermatogonia; Pre-L, pre-leptotene

spermatocytes. Quantification of the dispersion ratio of POLR1E or FBL is shown at right. Scale bars, 10 μm.

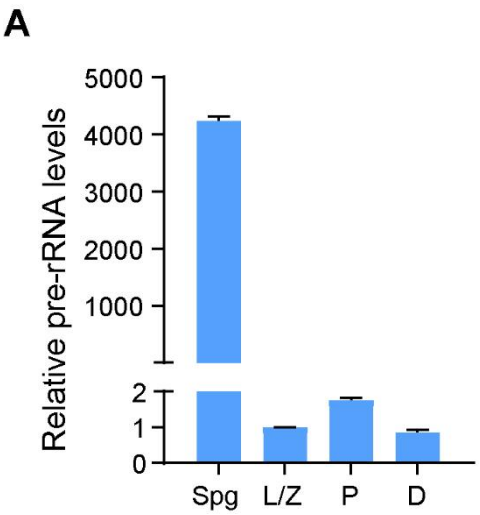

Figure S2 Stage-specific quantification of 47S pre-rRNA levels during meiotic prophase I.

Relative 47S pre-rRNA levels in L/Z, P, and D spermatocytes. 47S pre-rRNA transcript levels were detected by RT-qPCR. Data are presented as mean ± SEM (n=3 biological replicates). Spg: spermatogonia; L/Z: leptonema/zygonema; P: pachynema; D: diplonema.

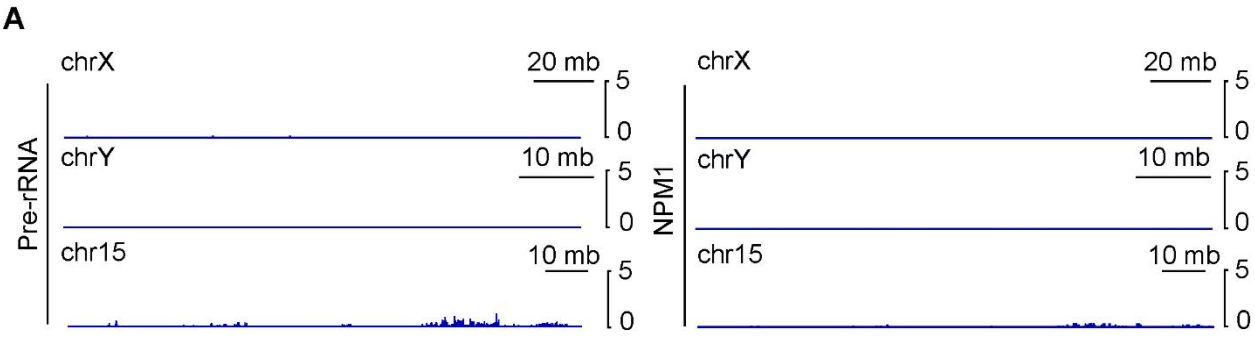

Figure S3 Chromatin-binding profiles of pre-rRNA and NPM1 in leptotene/zygotene spermatocytes.

Genome-wide distribution heatmaps showing ChIRP-seq (pre-rRNA) and CUT&Tag-seq (NPM1) signals at the indicated genic regions.

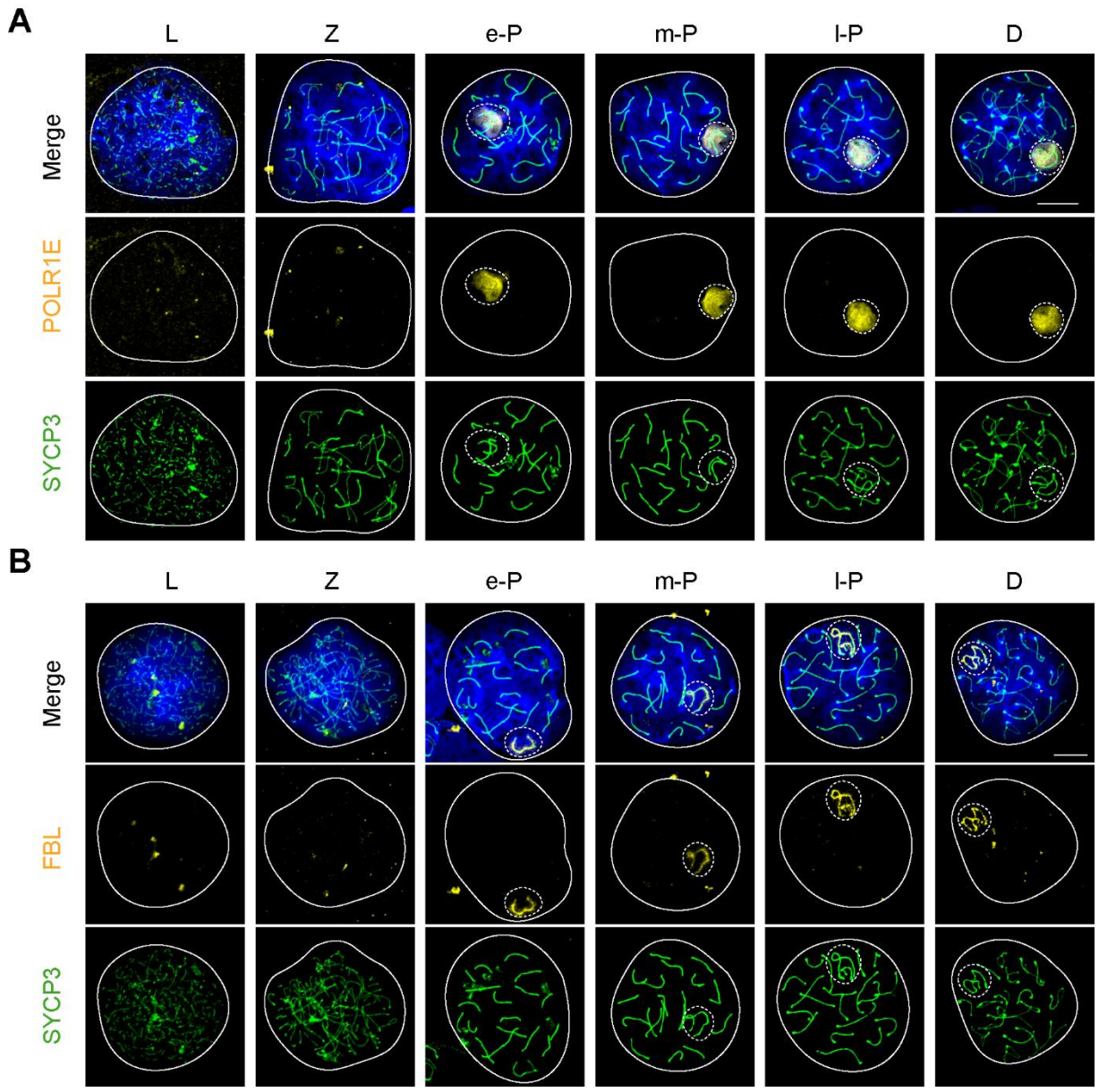

Figure S4 Nucleolar components dynamically fuse with the XY body during meiotic prophase I.

Distribution of the nucleolar proteins POLR1E **(A)** and FBL **(B)** from leptotene to diplotene. Representative images of POLR1E and FBL staining are shown. L, leptotene; Z, zygotene; e-P, early pachytene; m-P, middle pachytene; l-P, late pachytene; D, diplotene. The XY body is indicated with dashed circles. Scale bars, 10 μm.

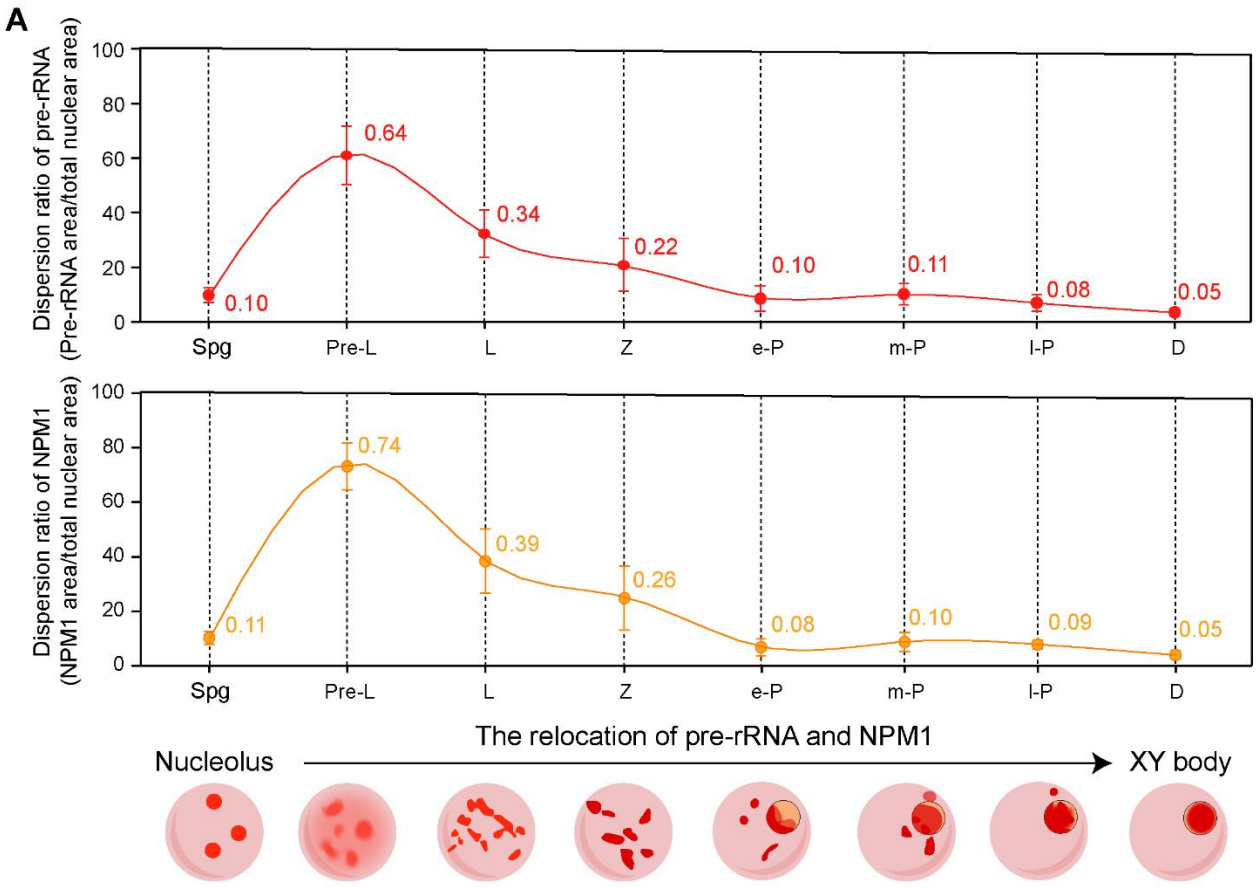

Figure S5 The relocation of nucleolar components from spermatogonia to diplotene spermatocytes.

Upper, statistical analysis of the dispersion ratio of pre-rRNA and NPM1 from spermatogonia to diplotene spermatocytes. Spg, spermatogonia; Pre-L, pre-leptotene spermatocytes; L, leptotene; Z, zygotene; e-P, early pachytene; m-P, middle pachytene; l-P, late pachytene; D, diplotene.

Lower, schematic summary of nucleolar component dynamics. Following nucleolar disassembly, the nucleolar components are reaggregated and fused into the XY body during meiotic prophase I.

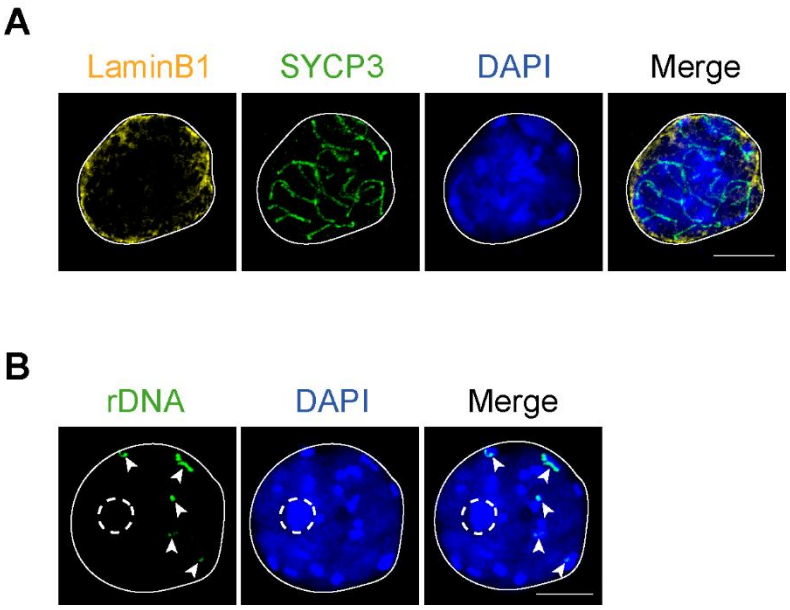

Figure S6 Detection of the nuclear envelope and rDNA loci in pachytene spermatocytes.

(A) Detection of the nuclear envelope by LaminB1 immunostaining.

(B) Detection of rDNA loci by DNA FISH. White arrows indicate rDNA signals. The XY body is indicated with dashed circles.

Scale bars, 10 μm.

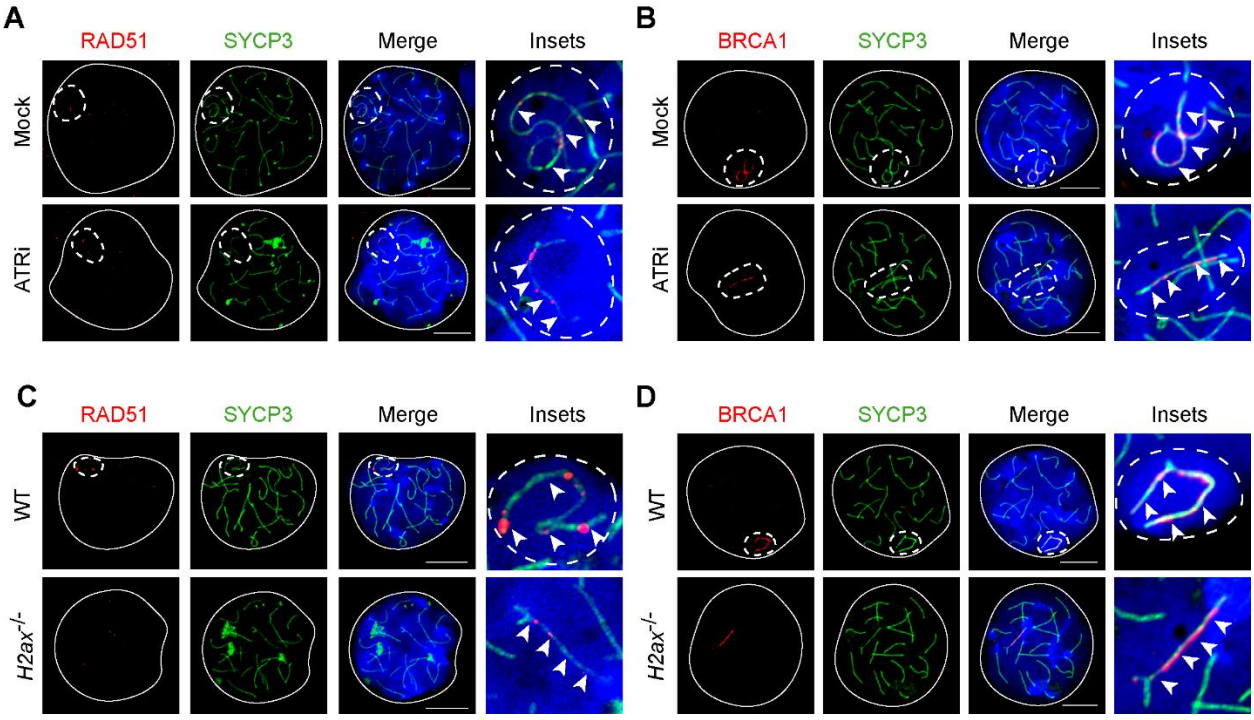

Figure S7 Persistent RAD51 and BRCA1 signals on the sex chromosomes in ATR-inhibited or *H2ax* KO pachytene spermatocytes.

(A, B) RAD51 and BRCA1 are still localized on the elongated X chromosome after ATR inhibition in pachytene spermatocytes. Pachytene spermatocytes were treated with the ATR inhibitor AZ20 (10 μM, 24 h). The distribution of RAD51 (A) and BRCA1 (B) was detected by immunostaining. The XY body is indicated with dashed circles. Sex chromosomes are indicated by arrows.

(C, D) RAD51 and BRCA1 are still localized on the elongated X chromosome in *H2ax* KO pachytene spermatocytes. The distribution of RAD51 (C) and BRCA1 (D) in WT and *H2ax* KO pachytene spermatocytes was detected by immunostaining. Sex chromosomes are indicated by arrows.

Scale bars, 10 μm.

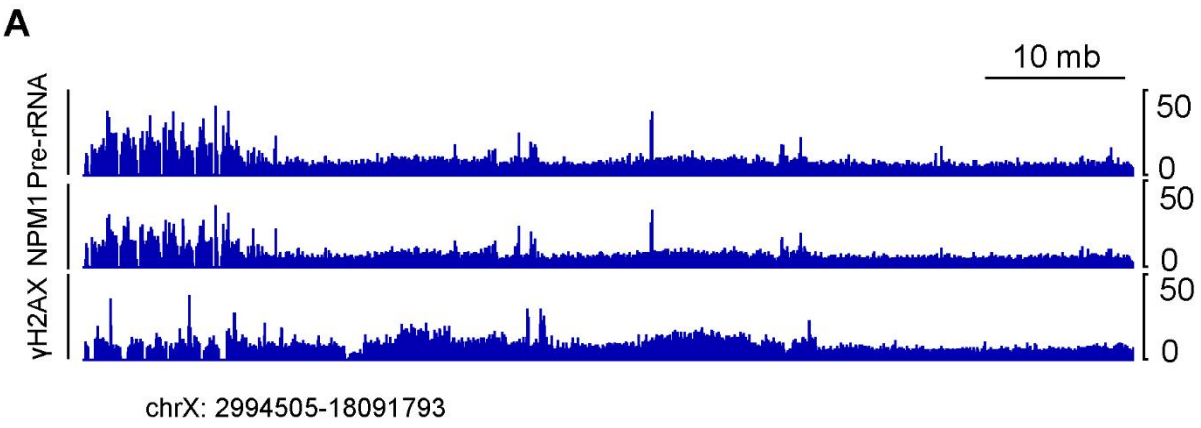

Figure S8 Chromatin-binding profiles of pre-rRNA, NPM1, and γH2AX in pachytene spermatocytes.

Genome-wide distribution of pre-rRNA, NPM1, and γH2AX on the X chromosome in pachytene spermatocytes.

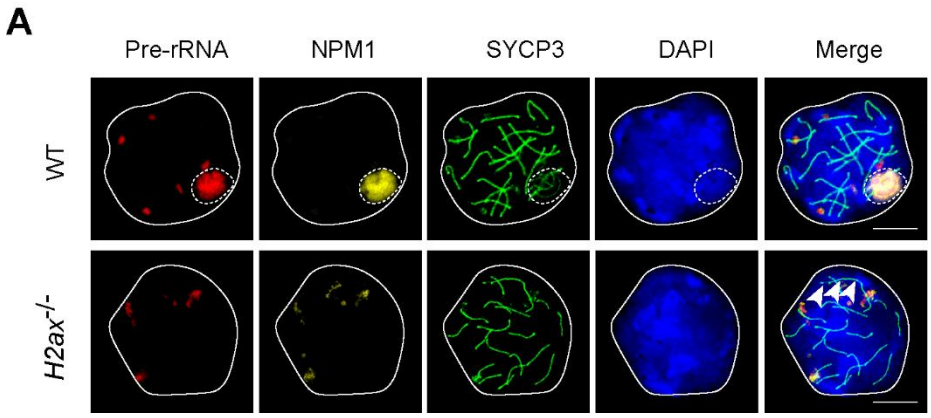

Figure S9 Detection of the pre-rRNA and NPM1 in WT and *H2ax* KO pachytene spermatocytes.

The distribution of pre-rRNA and NPM1 in WT and *H2ax* KO pachytene spermatocytes was detected by IF-FISH. Sex chromosomes are indicated by arrows. Scale bars, 10 μm.

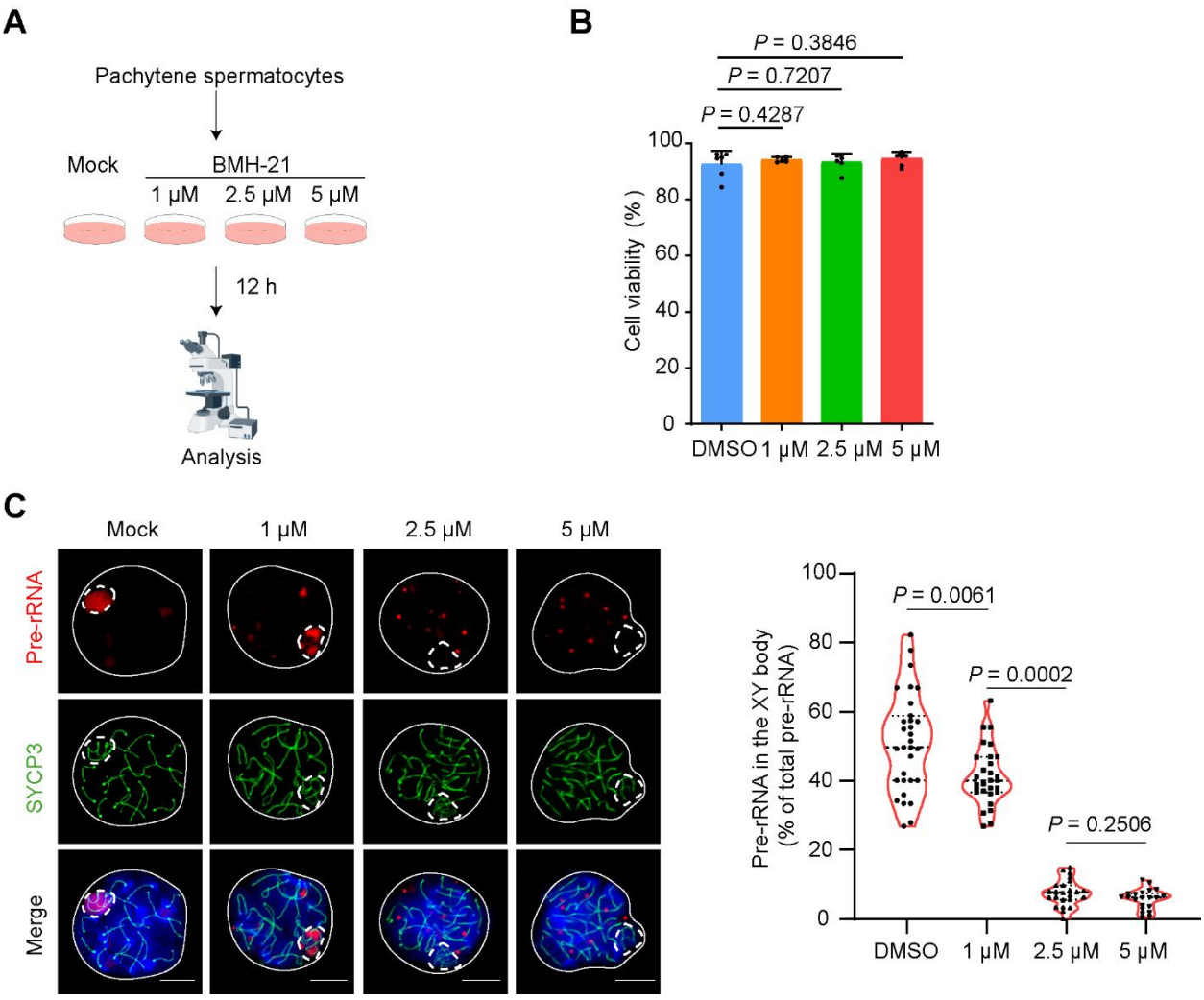

Figure S10 BMH-21 releases pre-rRNA from the XY body.

(A) Schematic workflow for the ex vivo drug treatment assay. Mouse pachytene spermatocytes were isolated by FACS and were then cultured with the indicated concentration of BMH-21 (12 h) for further analysis.

(B) Analysis of cell viability after BMH-21 treatment.

(C) Distribution of pre-rRNA after BMH-21 treatment. Representative images are shown at left. The XY body is outlined by dashed circles. Quantification of pre-rRNA localization in the XY body is shown at right. Scale bars, 10 μm.

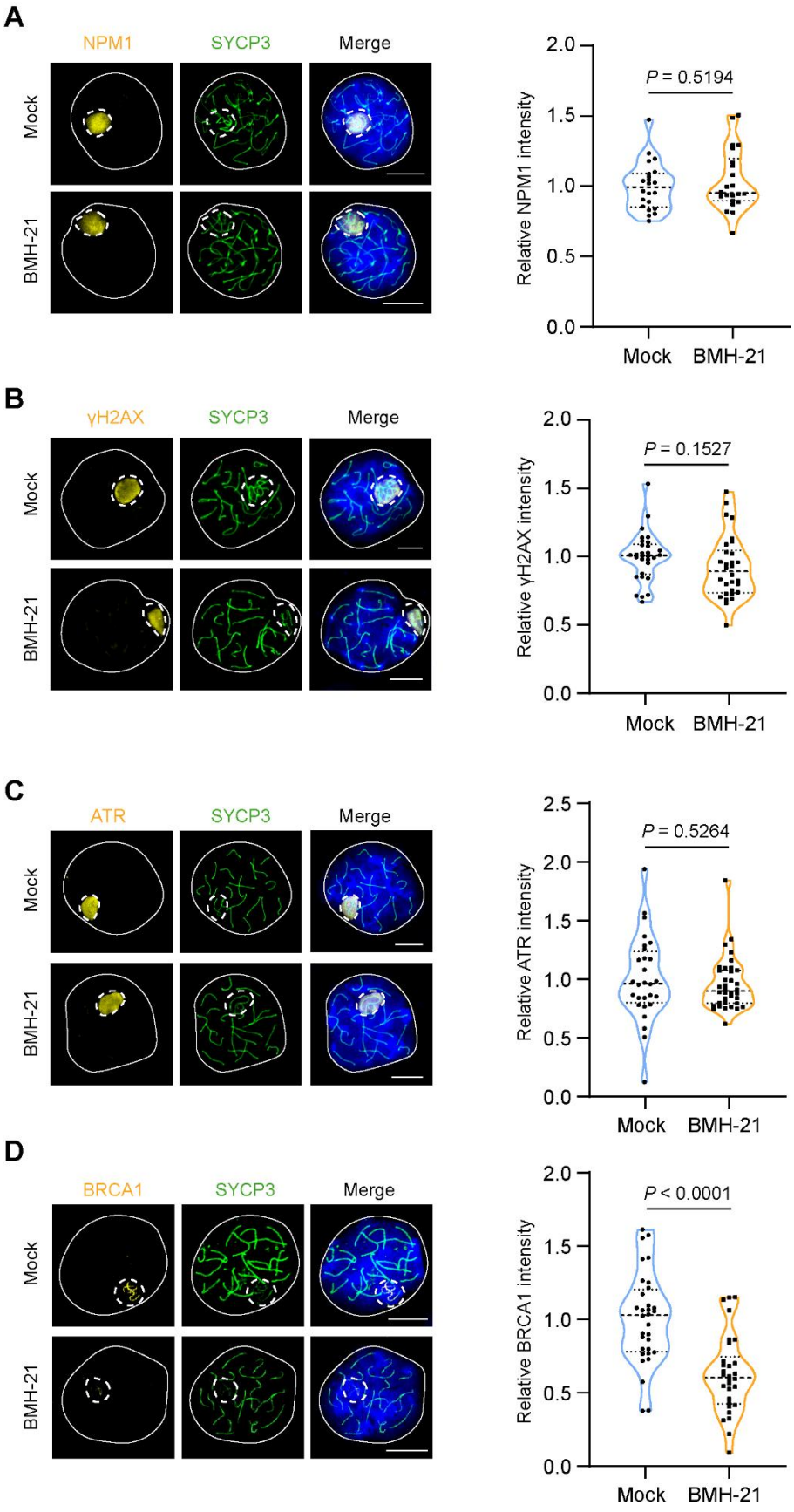
A
NPM1
SYCP3
Merge
Mock
BMH-21
Relative NPM1 intensity
P = 0.5194
2.0
1.5
1.0
0.5
0.0
Mock
BMH-21
B
γH2AX
SYCP3
Merge
Mock
BMH-21
Relative γH2AX intensity
P = 0.1527
2.0
1.5
1.0
0.5
0.0
Mock
BMH-21
C
ATR
SYCP3
Merge
Mock
BMH-21
Relative ATR intensity
P = 0.5264
2.5
2.0
1.5
1.0
0.5
0.0
Mock
BMH-21
D
BRCA1
SYCP3
Merge
Mock
BMH-21
Relative BRCA1 intensity
P < 0.0001
2.0
1.5
1.0
0.5
0.0
Mock
BMH-21

Figure S11 Differential effects of BMH-21 on the localization of XY body-associated factors. Analysis of γH2AX (A), NPM1 (B), ATR (C), and BRCA1(D) in pachytene spermatocytes with or without BMH-21 treatment (2.5 μM, 12 h). Representative images are shown at left. The XY body is outlined by dashed circles. Quantification of relative γH2AX, NPM1, ATR, and BRCA1 signal intensity in the XY body is shown at right. Scale bars, 10 μm.

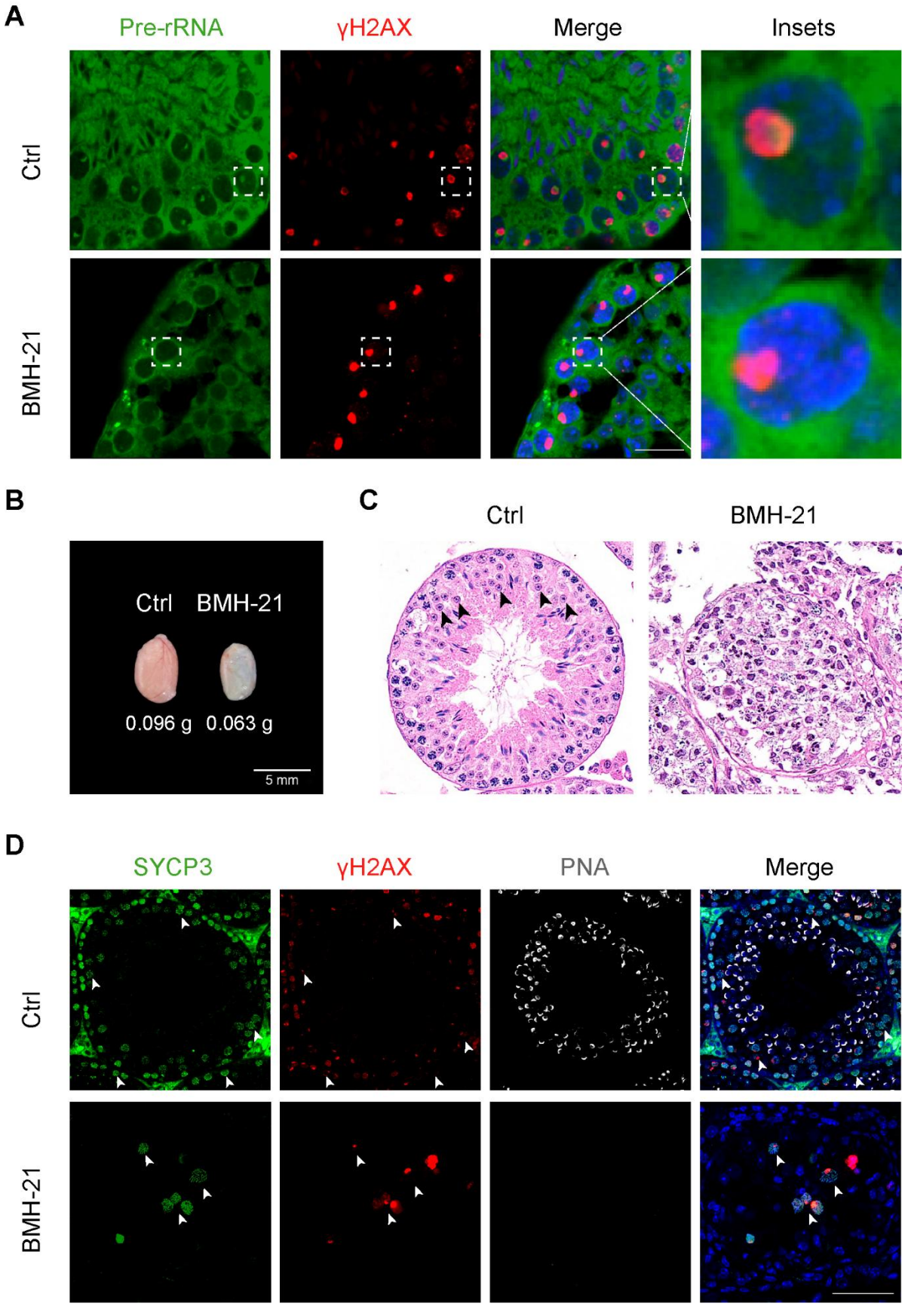
A
Pre-rRNA
γH2AX
Merge
Insets
Ctrl
BMH-21
B
Ctrl
BMH-21
0.096 g
0.063 g
5 mm
C
Ctrl
BMH-21
D
SYCP3
γH2AX
PNA
Merge
Ctrl
BMH-21

Figure S12 Pre-rRNA is required for spermatogenesis.

BMH-21 (10 μL, 50 uM) was administered into one testis of the mouse by rete testis microinjection, while the vehicle solution was injected into the contralateral testis.

(A) Examination of pre-rRNA in the XY body.

(B) Representative pictures of the testes.

(C) H&E staining of the testes. Round spermatids are indicated by arrows.

(D) Immunostaining of testis sections. Pachytene spermatocytes were identified based on SYCP3 and γH2AX staining and are indicated by arrows. PNA-positive cells denote haploid spermatids. Scale bar, 50 μm.